Hγ and Hδ Absorption Features in Stars and Stellar Populations

Guy Worthey[1]
Department of Astronomy, University of Michigan, Ann Arbor, MI 48109-1090

D. L. Ottaviani[2]
Department of Astronomy, University of Michigan, Ann Arbor, MI 48109-1090

ABSTRACT

The Hγ and Hδ absorption features are measured in a sample of 455 (out of 460 original Lick/IDS) stars with pseudo equivalent width indices. For each Balmer feature, two definitions involving a narrow ($\sim$ 20Å) and a wide ($\sim$ 40Å) central bandpass were measured. These four new Balmer indices augment 21 indices previously determined by Worthey et al. (1994), and polynomial fitting functions are provided which give index strengths as a function of stellar temperature, gravity, and [Fe/H]. The new indices are folded into models for the integrated light of stellar populations and predictions are given for single-burst stellar populations of a variety of ages and metallicities. Contrary to initial hopes, the indices cannot break a degeneracy between burst age and burst strength in post-starbust objects, but they are successful mean age indicators when used with sensitive metallicity indicators. An appendix gives data, advice, and examples of how to transform new spectra to the 25-index Lick/IDS system.

Subject headings: stars: abundances - stars: fundamental parameters - galaxies: evolution - galaxies: stellar content

1. Introduction

Determining the ages of old stellar populations is complicated by the similar effects that age and metallicity have on the integrated spectral energy distribution (O'Connell 1994, Worthey 1994). In order to maximize sensitivity to both age or metallicity, it is advantageous to examine individual absorption features at high spectral resolution. Although not completely immune to metallicity effects in integrated light, Balmer lines are less sensitive to metals because they depend mostly on the behavior of the main sequence turnoff temperature with age and metallicity rather than the behavior of the red giant branch temperature. Younger, more massive main sequence

---

[1]Hubble Fellow

[2]Present Address: Materials Science and Engineering, North Carolina State Univ., Raleigh, NC 27695

stars are hotter and have strong hydrogen absorption. Metal poor populations also have hotter main sequence stars, but the effect is somewhat muted compared to age. The difference of age-metal sensitivity between Balmer lines and metallic absorption features that key mostly to the red giant branch means that mean age and mean metallicity can be found simultaneously given appropriate stellar population models (Worthey 1994).

The Hβ feature has been studied in the past (O'Connell 1976, 1980; Burstein et al. 1984; González 1993; Faber et al. 1994) with possible age sensitivity in mind, but González (1993) finds that nebular emission, present at a measurable level in most early type galaxies, can fill in the Hβ absorption readily, making an accurate measurement of the true absorption difficult. Because lower order Balmer lines are affected more strongly by emission from ionized gas (e.g. Osterbrock 1989) attention by the community is broadening to include higher order Balmer lines (Rose 1985, 1994; Jones & Worthey 1995; Worthey 1996) .

In this paper we measure Hδ and Hγ each with a narrower ($\sim$20Å; "F"-definition) and a wider ($\sim$40Å; "A"-definition) central bandpass so there are four indices measured in total. The "A" means that the wider definition measures most of the absorption present in A-type stars, and the narrower "F" catches most of the absorption in F-type stars but begins to "fall in" to the very wide profile of an A star. This is illustrated in Figure 1. The reason for exploring different sizes of indices is manifold. Wider indices have smaller measurement errors in the case where photon statistics are important. Also, velocity dispersion in elliptical galaxies makes narrow absorption features hard to measure: the practical limit to the width of a measurable feature is something like 5 to 10Å in the optical for large galaxies because the correction factor back to zero velocity dispersion becomes greater than a factor of two. From these considerations, wider indices are clearly better. However, wide indices can throw away valuable information. For instance, Jones & Worthey (1995) exploit extremely narrow Hδ and Hγ definitions to achieve extraordinary sensitivity to population age. The desire to reliably investigate large galaxies drives us to consider wider indices, but the uncertainty of the outcome drives us to test different widths.

The four indices for two Balmer lines were measured in a library of stars with atmospheric parameters taken from Worthey et al. (1994), and the behavior of the indices with temperature, gravity, and [Fe/H] is summarized with fitted polynomials. The polynomial predictions are then used to predict index values for stars along evolutionary isochrones and these values are summed and expressed as indices for *populations* of different ages and metallicities. This work is precursor calibration to an observational project undertaken at Michigan-Dartmouth-MIT observatory to obtain good quality spectra of a large sample of early-type galaxies, to which the models will be compared. This work extends that of Worthey et al. (1994) and Worthey (1994), which papers followed the behavior of 20 metallic absorption features plus Hβ in stars and incorporated them into stellar population models.

The observations and measurement of the indices are discussed in §2, followed by a description of the polynomial fits and the insertion of the polynomials into population models in §3. A few implications and extensions are discussed in §4. An appendix discusses the successful transformation from new CCD data to the Lick/IDS system, advice which applies to all 25 indices.

2. Observations

The stellar spectra were obtained from 1972 to 1984 using the red-sensitive image dissector scanner (IDS) and Cassegrain spectrograph on the 3m Shane telescope at Lick Observatory. The spectra ranged from about 4000 to 6400 Å, with a resolution of 8 to 10 Å (see appendix). The spectra were not fluxed, but were divided by the spectrum of a quartz-iodide tungsten lamp. K giant line strength standard stars were observed nightly to enable time-invariant line strength calibration. A complete description of the observational method is given in Burstein et al. (1984), Faber et al. (1985), and Trager et al. (1997). However, the methods of index measurement (using cross-correlation to remove wavelength shifts) in this paper are essentially identical to those of Worthey et al. (1994).

Absorption feature indices are composed of measurements of relative flux in a central "feature" bandpass and two flanking "pseudocontinuum" bandpasses as illustrated in Figure 1. Once the average flux in the pseudocontinuum bandpasses are found, a line is drawn between their midpoints to represent the "continuum" from which an index is measured by integration within the "feature" bandpass and expressed in terms of an equivalent width (EW). The wavelength definitions of the four Balmer indices are given in Table 1. The Table 1 wavelengths are good to 0.3 Å RMS, based on cross-correlation with CCD spectra taken at MDM observatory with a wavelength calibration more solid than that delivered by the Lick/IDS setup.

The spectra were automatically measured by a computer program that was built to deal with the quirks of Lick/IDS data. In brief, after an initial pass to roughly calibrate the wavelength based on the positions of strong absorption features, 1-3Å localized wavelength shifts (present in Lick/IDS data) were removed with an automatic cross-correlation routine that uses template stars at different temperatures (three templates were used) to estimate the wavelength shifts in

Table 1. Index Definitions

	Name	Index Bandpass	Blue Bandpass	Red Bandpass	Units	Error
01	Hδ_A	4083.50 - 4122.25	4041.60 - 4079.75	4128.50 - 4161.00	Å	±0.64
02	Hγ_A	4319.75 - 4363.50	4283.50 - 4319.75	4367.25 - 4419.75	Å	±0.48
03	Hδ_F	4091.00 - 4112.25	4057.25 - 4088.50	4114.75 - 4137.25	Å	±0.40
04	Hγ_F	4331.25 - 4352.25	4283.50 - 4319.75	4354.75 - 4384.75	Å	±0.33

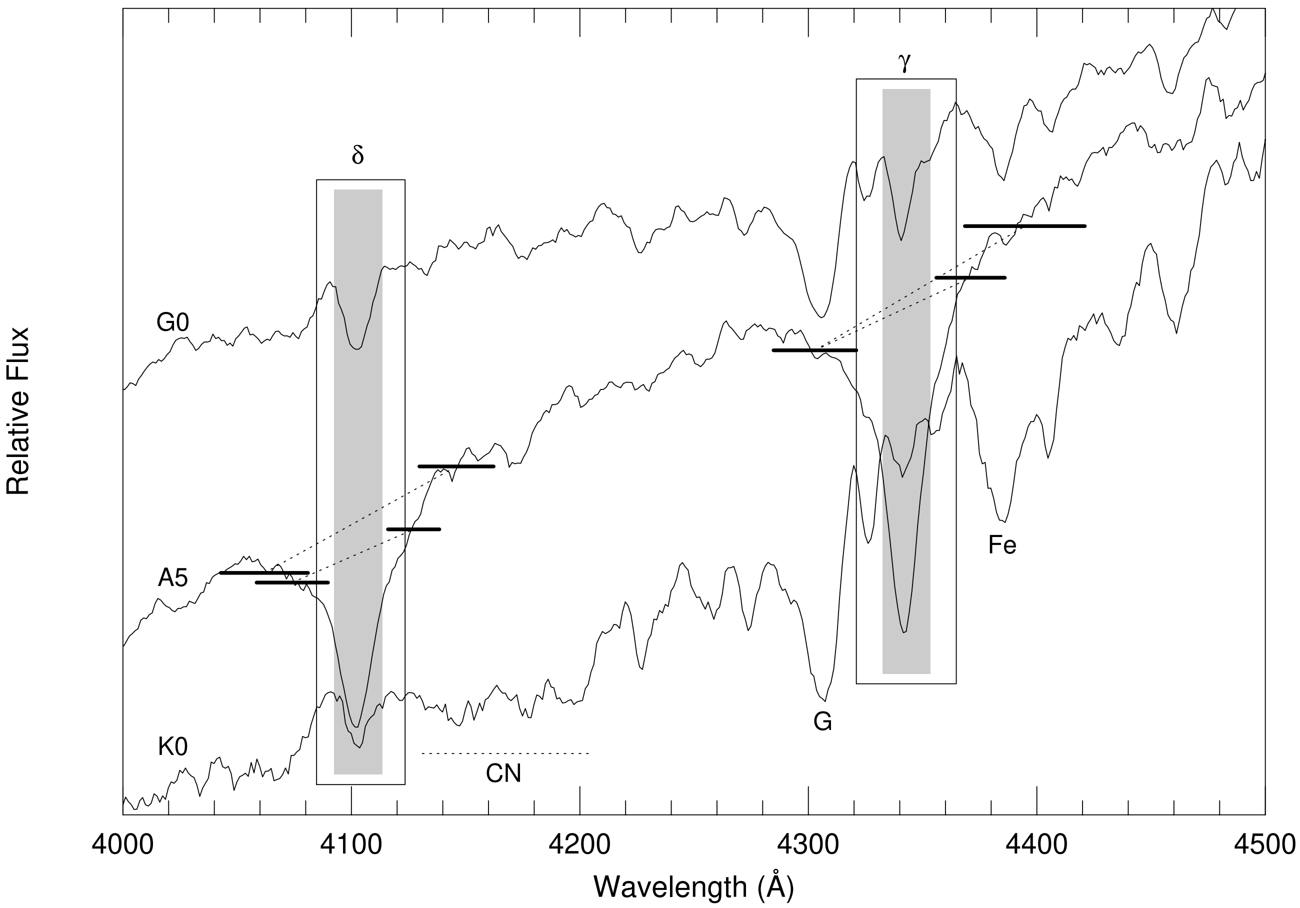

Fig. 1.— Representative stellar spectra are plotted with the definitions of all four Balmer indices shown. The flux scale is arbitrary and the spectra retain the instrumental response of the IDS (they are not flattened or fluxed). Stars of spectral type A5 V (HR 7141), G0 V (HR 660), and K0 III (HR 6018) are shown. The central passbands are shown as boxes, filled for the F-definitions, empty for the wider A-definitions. Pseudo-continuum sidebands are illustrated on the spectrum of the A-star as bold horizontal strokes at the approximate average flux level. The pseudocontinuum used for index measurement is drawn as a dashed line between flanking sidebands. The F-definitions have the narrower pairs. The blue-side sideband is the same for Hγ_F and Hγ_A. A few additional spectral features discussed in the text are marked.

the program objects. After automatic centering, the indices were measured. The raw indices for nightly-observed line strength standard stars were used to derive statistical "run corrections" that serve to correct for run to run differences in effective resolution, focus, and spectrum shape. These run corrections, if significant, were applied to the rest of the stars. Table 2 lists the final, fully corrected index values for the four definitions.

3. Model Indices

The steps between stellar index data and model integrated light indices could be accomplished in a variety of ways. The way we choose for the present is to fit the stellar data with arbitrary polynomial functions in which the index varies explicitly as a function of stellar temperature, metallicity, and gravity. These functions are coupled with population models (Worthey 1994) that start with stellar evolutionary isochrones and stellar fluxes that cover a range of age and metallicity. An assumed initial mass function gives the numbers of stars along the isochrone. The polynomial index fitting functions give the value of each index for each star along the isochrone. Weighted by the monochromatic luminosities and numbers of stars present, the index value for the whole population is produced.

The indices are fit using polynomial fitting functions which yield index strength as a function of effective temperature, log g, and [Fe/H]. Five sets of functions were fit in this manner; one for M type dwarfs (2800 K – 4400 K), one for M type giants (2300 K – 3900 K), one for cool stars (3570 K – 5160 K), one for warm stars (5040 K – 6720 K), and one for hot stars (6300 K – 13300 K). Cool stars were fit with polynomials in ($\log \Theta = \log(5040/T_{eff})$), log g, and [Fe/H], and warm stars with polynomials in Θ, log g, [Fe/H]. M type dwarfs and giants were fit with quadratics in $T_{\rm eff}$ alone, and the hottest stars were fit with polynomials in Θ, with a [Fe/H] term in two cases. The coefficients were found from a series of one-error least squares regressions in which the collection of χ^2 statistics were intercompared using the F-test to determine statistical significance. The number of observations and the quality of the data as listed in Table 2 were taken into account.

The adopted coefficients are listed in Tables 3 through 5 for all four indices. Tables 3 and 4 list coefficients only, but the polynomial is constructed in the straightforward manner. For example,

$$\mathrm{H}\delta_F = 47.273 - 86.425\Theta + 38.573\Theta^2 - 0.6310\Theta[\mathrm{Fe/H}] \qquad (1)$$

in the warm star temperature range. The RMS fit in terms of the assumed observational errors is also given in Tables 3 and 4. The fit errors are a little larger than the observational errors. For Hδ definitions the RMS numbers give a hint that hotter stars have smaller measurement errors than was inferred from the (K giant) line strength standard stars. We judge this effect to be real, and probably a result of higher count rates in the blue for hotter stars.

The implementation of the polynomial index predictions into the population models is

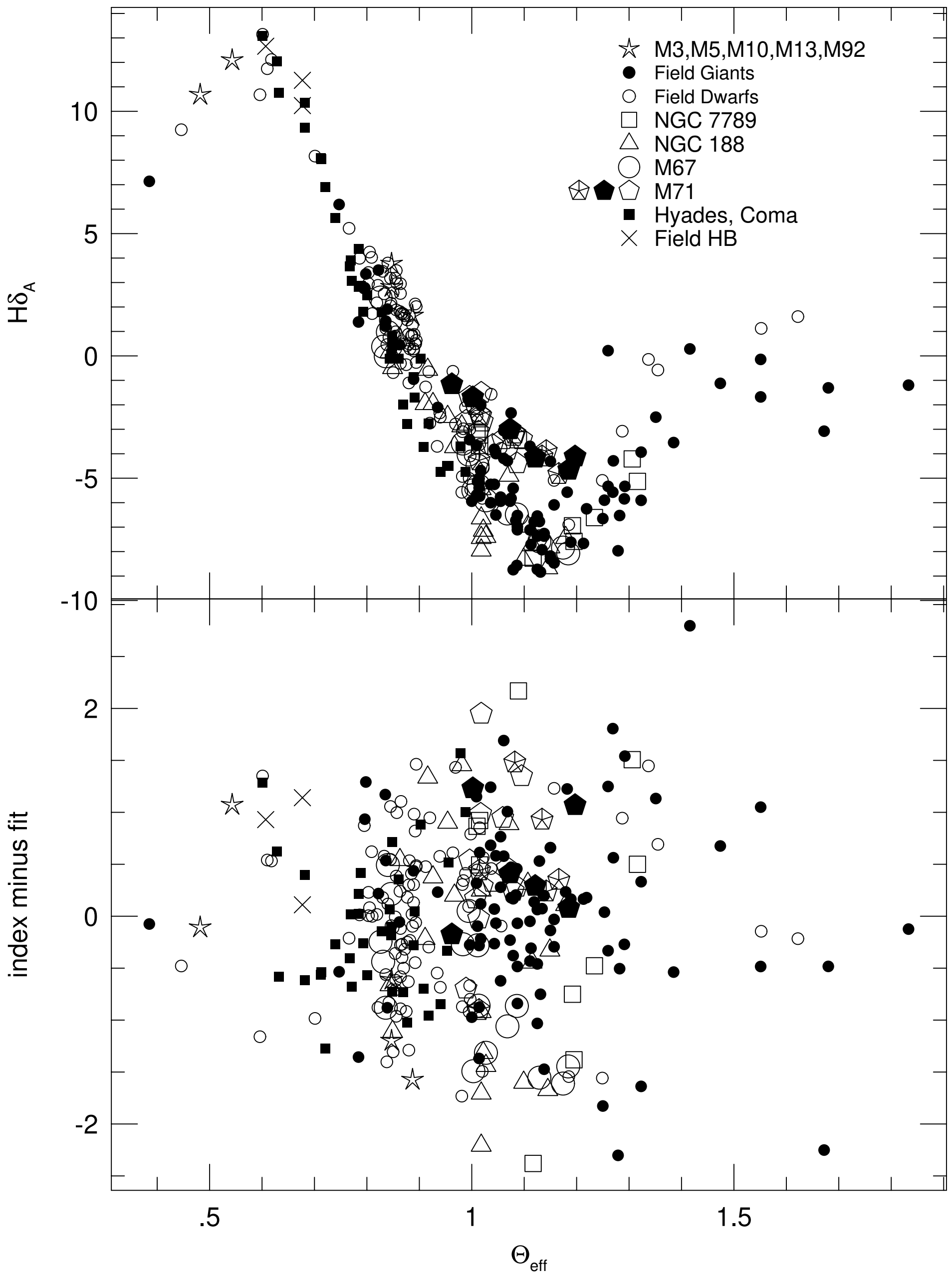

Fig. 2.— (upper panel) The behavior of Hδ_A with temperature variable $\Theta_{eff} = 5040/T_{eff}$ in stars of different environments as given in the symbol key. The symbols for M71 stars are solid if they are CN-strong (6 stars), starred if they are CN-weak (6 stars). (lower panel) The index residuals left after the polynomial fits (given in tables 3-5) are subtracted. The residuals reflect both observational index error and errors in assumed temperature, metal abundance, and gravity.

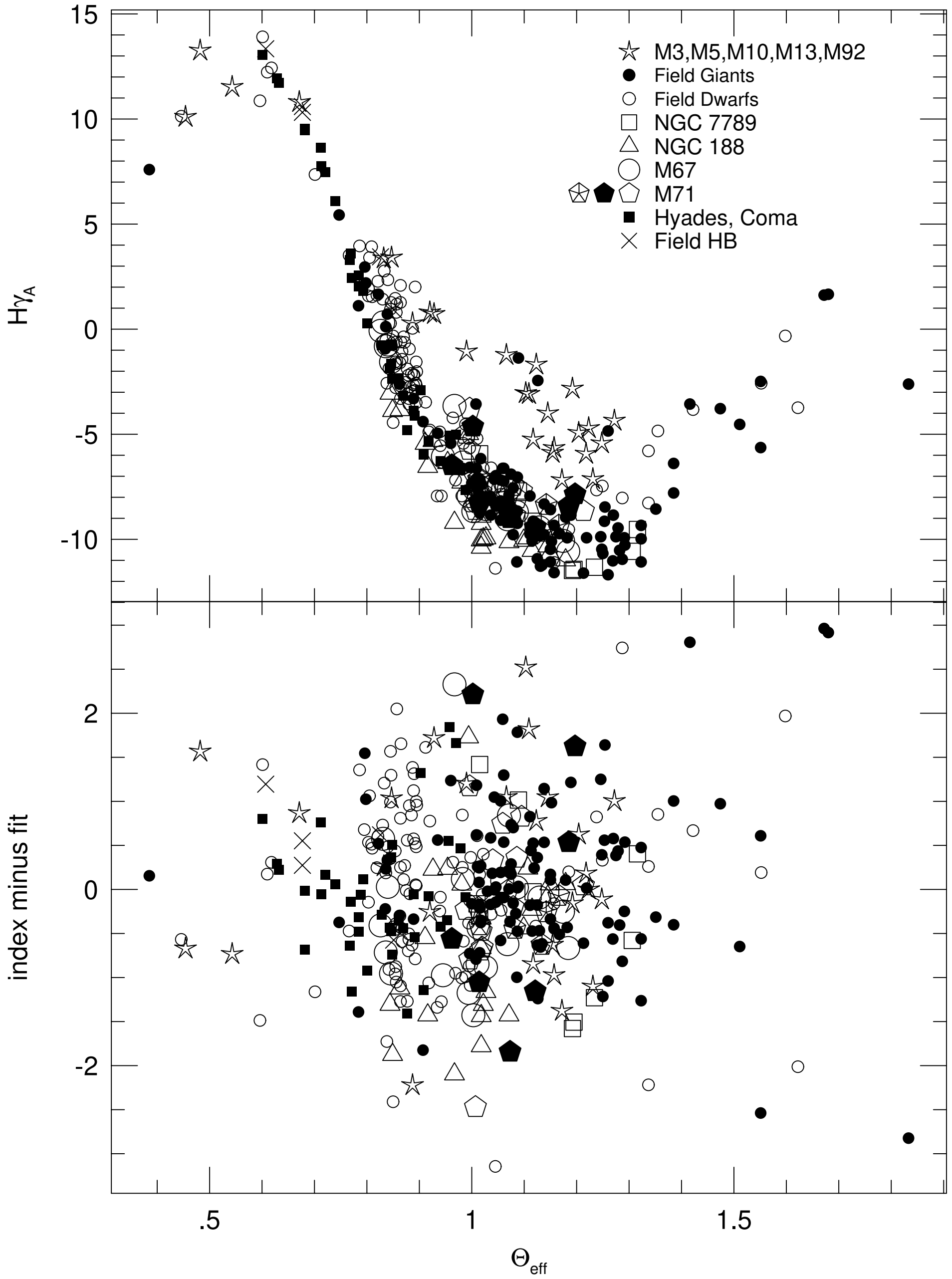

Fig. 3.— Index behavior as in Fig. 2, but for $H\gamma_A$. More globular cluster stars appear at low temperature because in most runs that observed globular cluster stars the spectrograph translation was such that the blue end of the spectrum was cut off.

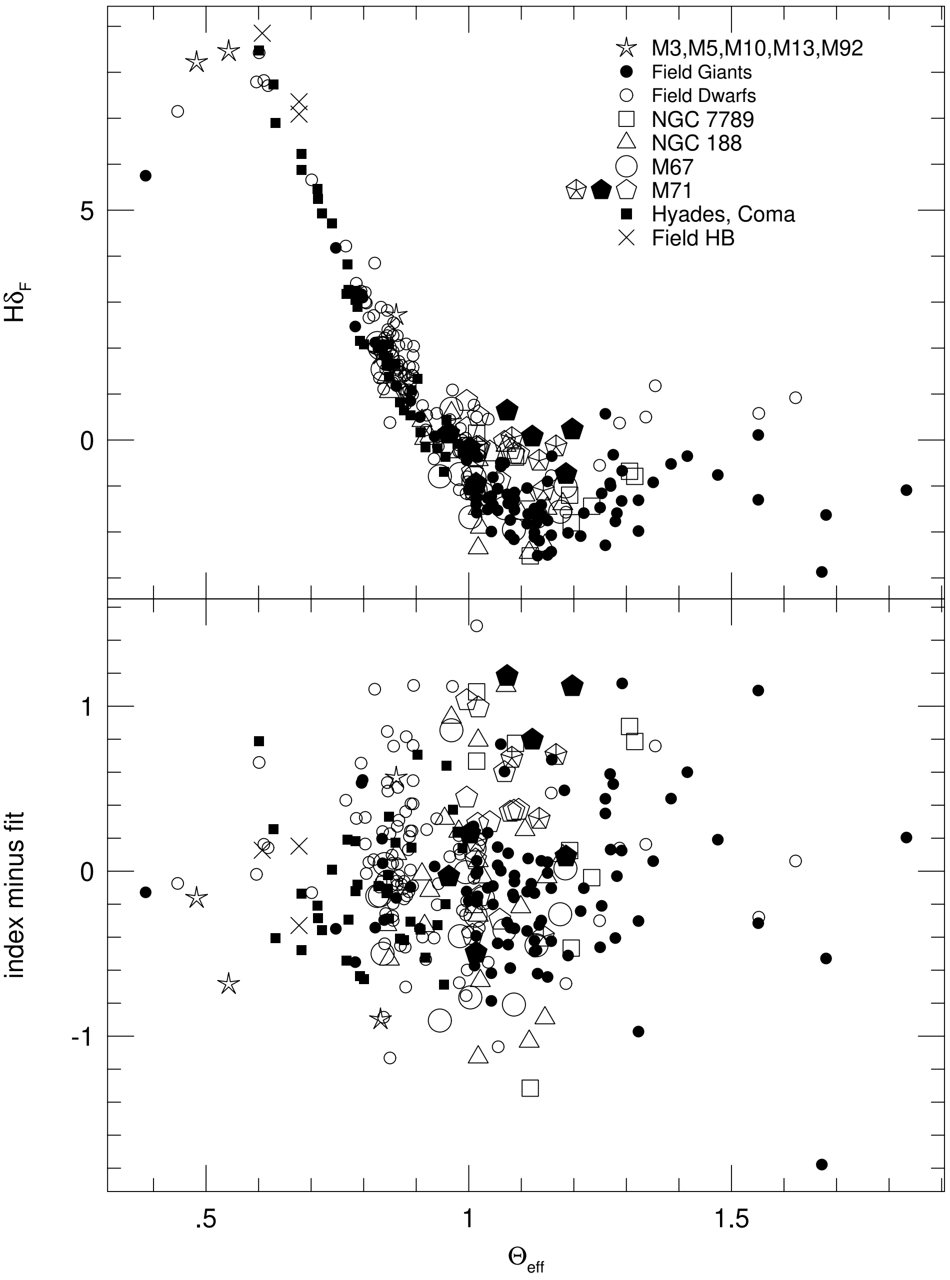

Fig. 4.— Index behavior as in Fig. 2, but for $H\delta_F$.

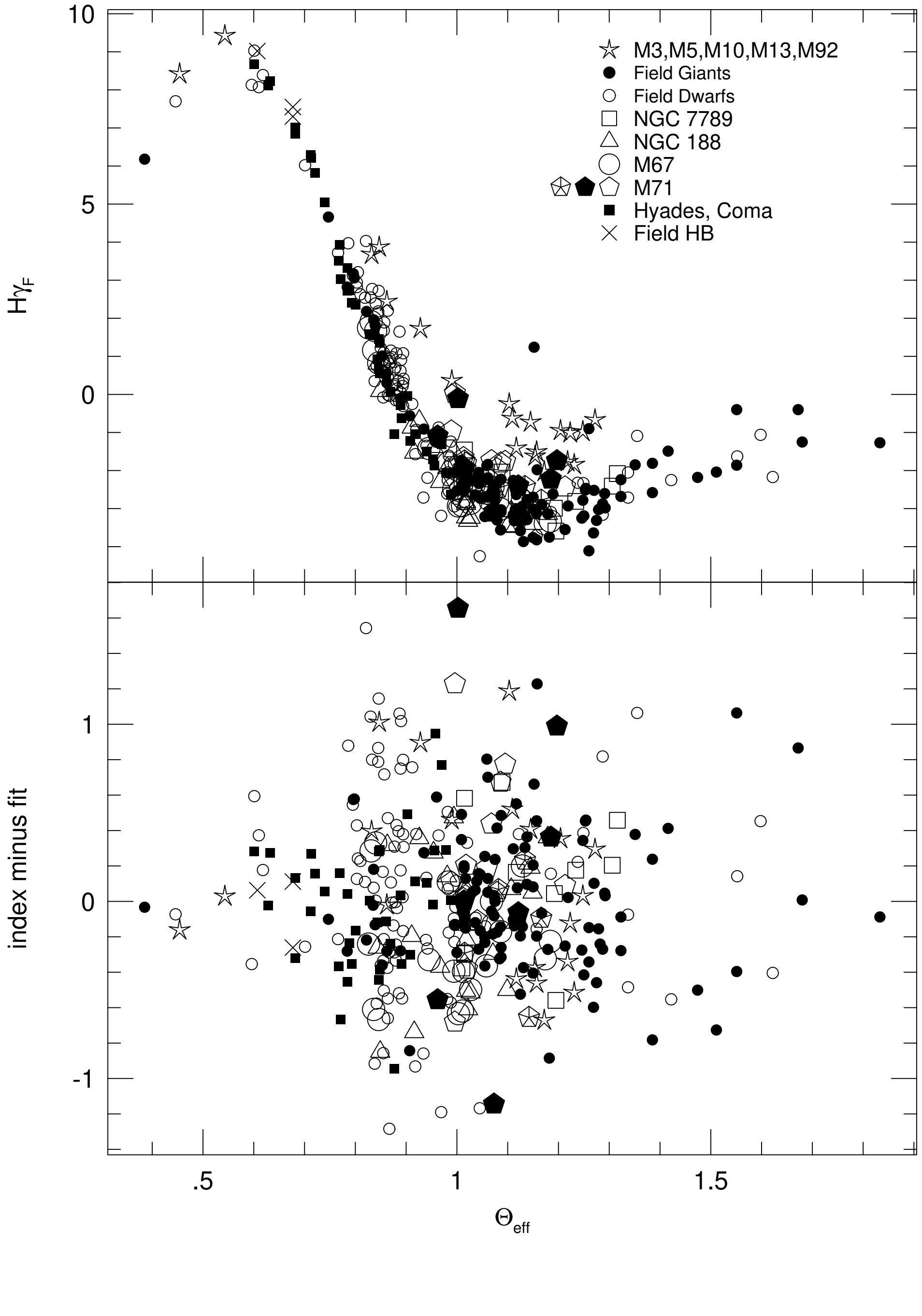

Fig. 5.— Index behavior as in Fig. 2, but for $H\gamma_F$. More globular cluster stars appear at low temperature compared to Fig. 2 because in most runs that observed globular cluster stars the spectrograph translation was such that the blue end of the spectrum was cut off.

identical to that in Worthey (1994), to which the reader is referred for tests of model reliability and a more detailed description of the construction of the models. In brief, the models begin with a compilation of VandenBerg isochrones (VandenBerg 1985; VandenBerg & Bell 1985; VandenBerg & Laskarides 1987) and revised Yale isochrones (Green, Demarque, & King 1987) combined with 1992 Kurucz model fluxes for stars. Other sources of data were used; please refer to Worthey (1994). Assuming a Salpeter (1955) power-law IMF, the run of mass along the isochrone translates into numbers of stars. For each bin on the isochrone, the number of stars is computed and a flux F_λ is associated with that bin, multiplied by the bolometric luminosity of the bin and by the number of stars in the bin. Treating the theoretical F_λ just as one would a real spectrum, at the Table 1 wavelengths the pseudocontinuum levels are found and a straight line is drawn. The value of F_λ at the midpoint of the feature bandpass is adopted as "$F_{\rm C}$," the "continuum" flux. The polynomials in Tables 3–5 give the index value, from which the flux in the index passband $F_{\rm I}$ is computed ($F_{\rm I}$ is the continuum flux minus the absorption). After summing $F_{\rm C}$ and $F_{\rm I}$ over each bin in the isochrone, the indices are then re-expressed as equivalent widths

$$\text{Index} = (\lambda_2 - \lambda_1)(1 - F_{\rm I}/F_{\rm C}) \tag{2}$$

measured in Å, where $(\lambda_2 - \lambda_1)$ is the width of the feature bandpass (Table 1) used to measure the index. Model predictions for globular-cluster-like populations for which a single age and metallicity are present are listed in Table 6 and illustrated in Figure 6 for all four Balmer indices.

4. Discussion

Of primary concern is whether the Balmer indices are age-sensitive; the hope that initially spurred this investigation. We construct a metallicity sensitivity parameter from the model predictions of Table 6 (see footnote 4 in Worthey 1994 for the exact prescription) which is the partial derivative (d log Age / d log Z) taken at constant index. The parameter represents the age change needed to balance a metallicity change so that the index remains constant. The Z-sensitivity parameter is listed in Table 7 for the new indices and a few others from Worthey (1994) for comparison. A larger number indicates a greater metallicity sensitivity and thus a lesser age sensitivity. Of the Table 7 indices, Hβ is the most age sensitive, followed by Hγ_F, and so on. The new indices will be affected much less by Hydrogen emission than is Hβ, but due to their comparable age sensitivity will provide independent measures of mean population age. Note also that the A-definitions are a factor of two less sensitive to emission than the F-definitions due to the greater width of their feature passbands.

Adding the Table 7 results to those of Jones & Worthey (1995), there is a clear trend of Balmer line age sensitivity with index *width.* The Jones & Worthey "HR" indices are the narrowest possible, and show extraordinary age sensitivity. Table 7 indicates that the F-definitions are somewhat more sensitive than the A-definitions. Somewhat counter to this trend is the Hβ index. It is 29 Å wide, wider than the F-definitions, but still manages a greater age sensitivity due to

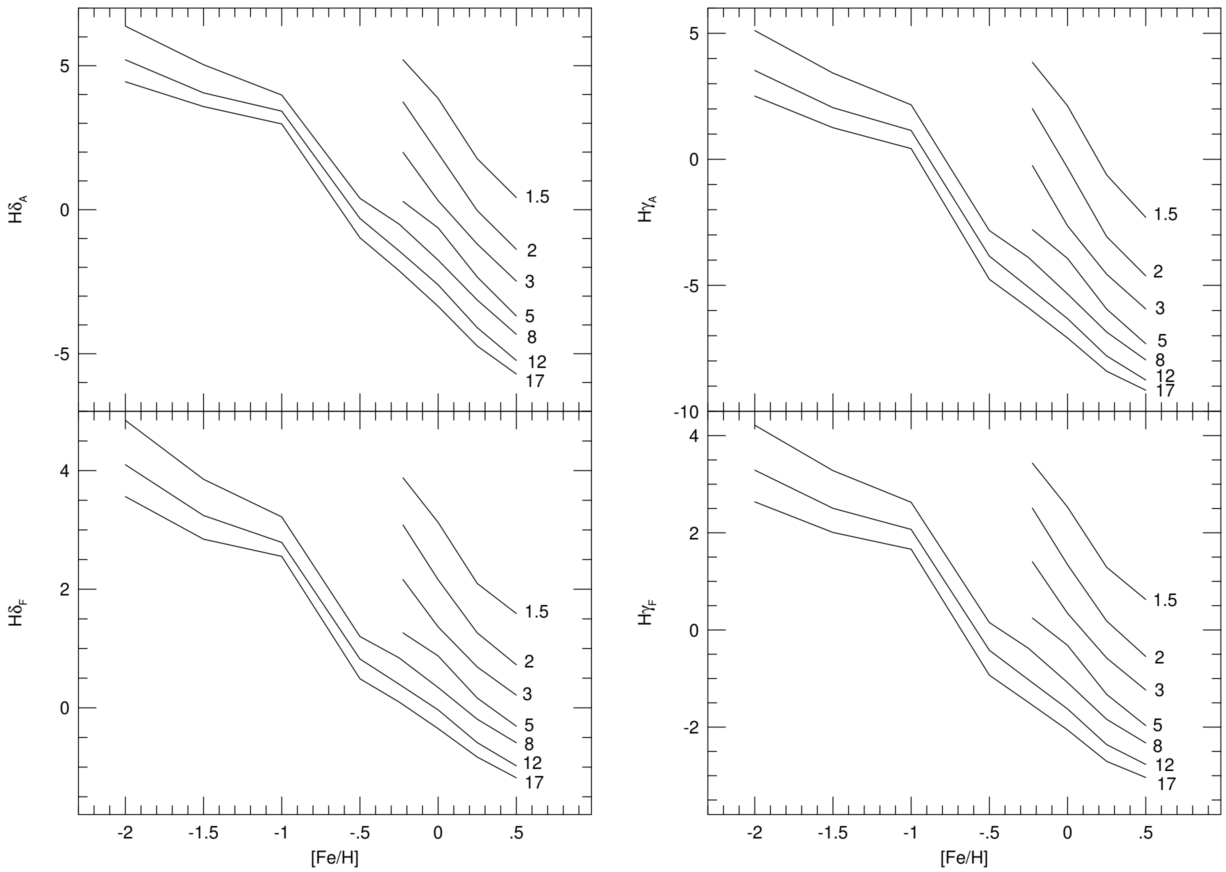

Fig. 6.— Model behavior for the four Balmer indices is shown as a function of population metallicity. Ages in Gyr are labeled next to the appropriate curves. All Balmer indices decrease with age and with metallicity. The jumps in index value between [Fe/H] = −1 and [Fe/H] = −0.5 are due to the horizontal branch morphology shifting from an extended M3-like branch to a red clump as metallicity increases. This shift of HB morphology was not included in the Worthey (1994) models.

the index's steep behavior with temperature. This behavior, in turn, may be a function of either Hβ's wavelength or the surrounding metallic absorption. The overall sensitivity/width trend is a valuable pointer toward designing an ideal age-sensitive index.

A secondary hope of the new Balmer indices was that they would provide some leverage for distinguishing between very recent bursts of star formation with relatively small amounts of mass involved and somewhat less recent bursts of star formation with relatively more mass involved, like the promising CaII indicator of Leonardi & Rose (1996). Small but youthful bursts can have exactly the same Balmer index *and* metallic index strengths as a larger, less youthful burst. To test whether or not the A-definitions have a behavior different than the F-definitions in these scenarios, we concocted different model mixtures that have the same location in any single Balmer-metal diagram of (1) a single (age,Z) pair and (2) several (age$_1$, age$_2$, Z_1, Z_2) quadruples that mimic the scenarios of small-but-young bursts superimposed on older populations that we are interested in disentangling. The result from these tests is that once a single Balmer index plus metal index combination is matched, the other Balmers matched within a fraction of an observational error. We tested only a small part of the (age,Z)^2 parameter space, but this is sufficient to show that most small-burst scenarios remain degenerate with single-age scenarios within the Lick/IDS index system. Continuing attention should be paid to finding reliable discriminators of the burst-age, burst-strength degeneracy.

The new Balmer indices are affected by abundance ratio effects, as are the previous 21 (Tripicco & Bell 1995). Abundance ratios are known to differ from the solar neighborhood mixture in other galaxies and in different places in our own galaxy (Wheeler, Sneden, & Truran 1989, McWilliam & Rich 1994, Worthey, Faber, & González 1992, Worthey 1996) and can have a profound effect on age determination (Worthey 1996). As indicated in Figure 1, the red pseudocontinua of both Hδ indices overlap cyanogen absorption, so an increase in N abundance will decrease the strength of the Hδ indices. Note that this effect is *not* clearly seen in the M71 giants plotted in Figures 2 to 5 whose CN strengths have been measured as "strong" or "weak" by Smith and collaborators (Smith & Norris 1982; Smith & Penny 1989; Penny et al. 1992; Briley et al. 1994). A small effect may be present but the errors in the M71 Lick data are larger than any signal. In addition, the shared blue pseudocontinuum of the Hγ indices lies squarely over the Fraunhofer G band, with absorption primarily due to CH, with lesser absorption from Ti and Fe. The Hγ indices are thus sensitive to C and O abundance (O because it determines how much C is free because of the large amount of C tied up in the CO molecule). In the near future, these effects will be quantified with model atmosphere calculations like those of Tripicco & Bell (1995). In addition to purely spectral effects, altered chemical mixtures also affect stellar lifetimes and, most especially, stellar temperatures as a function of evolutionary stage. These effects can also play havoc with age determinations (Worthey 1996).

Ongoing thanks goes to those who continue to maintain and improve the Lick/IDS data: Scott Trager, Deneyse Churchill, and Sandy Faber; and also to D. Burstein and J. J. González whose heroic past efforts started the Lick index industry. Karl Gebhardt generously provided his expertise and line-of-sight-velocity-distribution software, both of which were used for the appendix. Jim Rose is thanked for excellent referee suggestions. This work was supported by NASA through grant HF-1066.01-94A awarded by the Space Telescope Science Institute which is operated by the Association of Universities for Research in Astronomy, Inc., for NASA under contract NAS5-26555.

A. Transforming to the Lick/IDS system

Authors with spectral data that wish to use the population models or compare with previously published index data need to transform to the Lick/IDS system. The transformation needs to be done as securely as possible because the scientific results (mean ages, mean metallicities, abundance ratios) often depend on measuring indices at a level of accuracy where systematic effects are important. We provide this appendix as a guide for successful transformation. (It is not a "cook book" as there remains considerable room for creative improvement in these techniques. We do not wish to stifle such impulses!)

In the literature to date there are a few examples of transformation to the Lick/IDS system: González (1993) and Fisher, Franx, & Illingworth (1995) do perhaps the best job to date by artificially broadening their (star and galaxy) spectra with a gaussian of width such that the Lick system is approximately matched. Note that the wavelength span of these studies is roughly 4500-5500Å, which is only a fraction of the total span of the Lick spectra. This narrow wavelength range allowed González and Fisher et al. to apply a smoothing that was constant with wavelength (to be more precise, their smoothing was constant with $1/\lambda$, but the point is that the narrow wavelength range permits such approximations.) The resolution of the Lick/IDS spectra is known to degrade at the blue and red ends (Fig. 7). After one is able to match the stars very well and the indices are measured in the thus-transformed galaxy spectra, it is still necessary to correct for any additional stellar velocity dispersion in the galaxy data. The correction is to zero velocity dispersion on the Lick system, and can be readily calculated by finding a good template (a star or combination of stars) that matches the galaxy spectrum fairly well, artificially broadening the template to the observed dispersion of the galaxy, and measuring how the spectral indices change.

Of the various ways to transform to the Lick system, the most naïve, a straight linear transformation for stars in common, *we strongly recommend against* because it makes correcting for velocity dispersion effects in galaxies uncertain. A linear transformation may be adequate in the case where only stars are considered. In general, if the new data is at higher resolution than the ∼8–10 Å of the Lick/IDS data, it should be artificially broadened with a gaussian function until it best "matches", and this should yield the correct transformation *to within a small constant*. The residual constant will probably be due partly to systematic effects in the new data (such as incorrect broadening, incorrect index wavelength centering, bad sky subtraction, flat fielding errors) and also parly due to systematic effects in the Lick/IDS data. Operationally, the

Lick/IDS systematics are due to either spectral shape differences that will exist between new data and the Lick data, or to the various peculiarities of the Lick/IDS spectra that were dealt with by run-to-run corrections. The spectral shape effects should be negligible for narrow indices but possibly important for broad indices. The run correction procedure used for the Lick spectra may have caused some drift between the Lick system and reality, but we expect these additive drifts to be less than about half of the Lick measurement error, and hopefully almost negligible. We revisit this issue below.

A.1. IDS resolution as a function of wavelength

We used two sets of stellar spectra to find the resolution of the Lick stars. First, 70 exposures of 10 stars in common with Lick/IDS (mostly K giants) were taken from a 4-night run at Michigan-Dartmouth-MIT (MDM) observatory in October 1994 with spectra at about 5.1 Å FWHM resolution. Second, a recently published library of spectra (Jones 1996; also in Leitherer et al. 1996) at 1.8 Å FWHM in two regions: 3700-4500Å and 4700-5500Å has overlap of many stars with the Lick/IDS system and is approximately spectrophotometric.

Using these two sets of spectra, we first used Karl Gebhardt's nonparametric line-of-sight velocity distribution software, treating the higher resolution data as "template" and the Lick/IDS data as "galaxy." The conclusion from these tests is that the response of the Lick/IDS data *can* be treated as a gaussian. The Gauss-Hermite coefficients $h3$ and $h4$ (see Bender, Saglia, & Gerhard 1994 or van der Marel & Franx 1993) are of negligible size.

Next, we used a less sophisticated cross-correlation technique (see for instance Statler 1995) that assumes a gaussian instrumental profile. For every overlapping star we could find in the two samples the spectra were broken into ~200 Å chunks and the resolution needed to best match the Lick/IDS spectra was determined for each. The Lick/IDS resolution was then determined via $\sigma^2_{\rm IDS} = \sigma^2_{\rm CCD} + \sigma^2_{\rm smooth}$, where "CCD" refers to the resolution of the new spectra, and "smooth" refers to the width of the broadening function needed to reach the IDS system. The results are plotted in Figure 7. The implementation of the cross-correlation procedure was unexpectedly tricky, probably because of localized stretches and shifts in the Lick/IDS wavelength scale, which caused spuriously elevated χ^2 and thus made finding minima much more uncertain.

Finally, in a cruder way, we attempted to find the optimum resolution by finding the gaussian broadening that best reproduced the Lick/IDS *indices* that are sensitive to resolution effects. These are 3. Ca4227, 4. G, 5. Fe4383, 6. Ca4455, 7. Fe4531, 13. Mg b, 14. Fe5270, 15. Fe5335, 16. Fe5406, 17. Fe5709, and 18. Fe5782, but not all of these worked very well because of either nonmonotonic index behavior with increasing resolution or because of index insensitivity to resolution effects. The results are also displayed in Figure 7, and tend to confirm the results from cross-correlation, albeit with larger scatter.

The data used to make Figure 7 was also sorted as a function of Lick/IDS observing run to

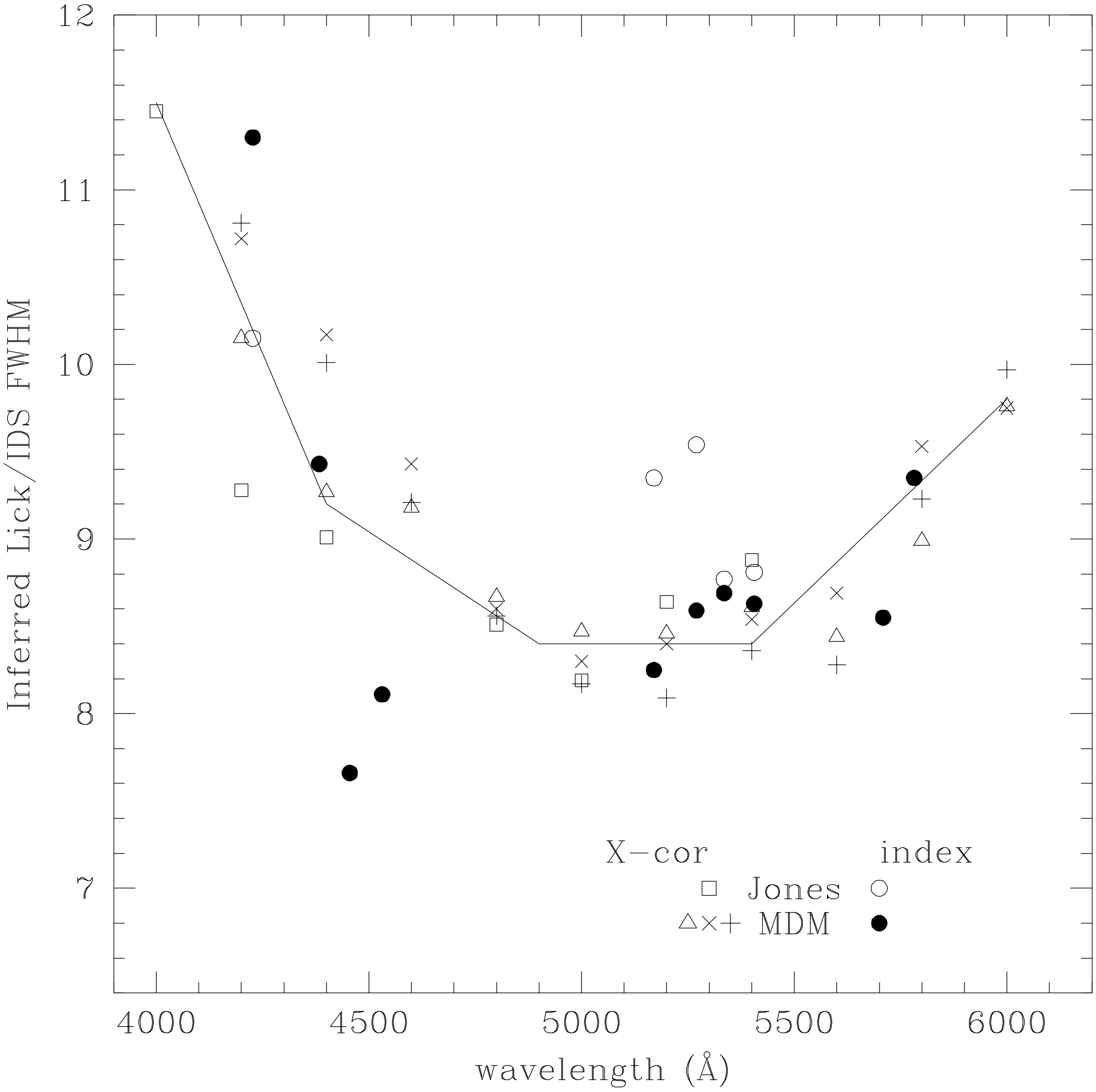

Fig. 7.— The inferred instrumental resolution of the Lick/IDS system from two stellar data sets described in the text: Jones and MDM. In the key, the symbols labeled “X-cor” are those values inferred from cross-correlation between overlapping stars, and the symbols labeled “index” are those values inferred from the cruder comparison of index values as a function of broadening. The line segments drawn are tabulated in table 8 and represent the authors’s by-eye current working guess. Uncertainty appears to be less than 5% redward of 4500 Å , but increases to 10% or more blueward.

look for time-dependent variation of resolution. In the middle of the spectrum the resolution was fairly stable with time. In the blue, it appears that the focus was somewhat worse for the early runs, but this does not matter much because usually the spectrograph was set to exclude the blue part of the spectrum in early runs. Another tentative conclusion from this test is that the origin of run-to-run index drifts in the narrower indices may be mostly due to changes in Lick/IDS instrument resolution. Especially convincing in this regard is run 61, the last IDS run, which is at better resolution than the others and had many significant run corrections. At the time the run corrections were applied it was not known why the run was deviant.

Note that Lick/IDS stellar spectra are available electronically via the URL http://astro.lsa.umich.edu/users/worthey along with current index wavelength definitions and the catalog of index values. The spectra retain all of their quirks of wavelength scale.

A.2. No stars in common with Lick/IDS?

When observing spectra from which Lick/IDS indices will be measured, it is vastly preferable to observe stars that are in the Lick library in order to have the most confidence that the system has been matched, but it should be possible to transform fairly well even if different stars were observed. We know of no examples in the literature where this has been attempted. The best broadening can be found from table 8. The size of the additive index shifts will be harder to estimate and probably cannot be done with precision. We would suggest making good guesses for the index strengths of the non-Lick stars, either by feeding stellar parameters into fitting functions (Worthey et al. 1994 or Gorgas et al. 1993) or by matching to Lick spectra of similar stars.

Some comments can be made on the expected size and direction of the additive constant correction by looking at table 9, which lists the median differences in index values after the new spectra were broadened to match the Lick/IDS system. For both sets of spectra, wavelength shift problems should be minimal: Jones spectra are wavelength calibrated to 0.2 Å or better, and the MDM spectra were cross-correlated with the Jones spectra to center them in wavelength.

For the very broad CN and Mg indices (not Mg *b*) we expect any shifts to be due to spectral shape differences. Jones spectra are approximately spectrophotometric, while the MDM spectra retain an overall instrumental response profile with wavelength. In agreement with unpublished experiments we have carried out on Lick spectra in combination with flux standards, the Jones shifts indicate that Lick/IDS Mg_1 and Mg_2 are essentially spectrophotometric. The MDM spectra, however, show a significant shift due to the way the spectrograph response curves in the middle of the spectrum. Both sets of spectra match the CN indices well.

For narrower indices it not so clear what causes the drifts. Troublesomely large shifts are MDM Ca4227, Jones G, Jones Fe4383, Jones Hβ, Fe5015, and the new Balmer indices. MDM Ca4227 can be discounted because the MDM intrumentral resolution is changing fast at that wavelength and we could easily be off by 10%, which would largely take care of the problem. The

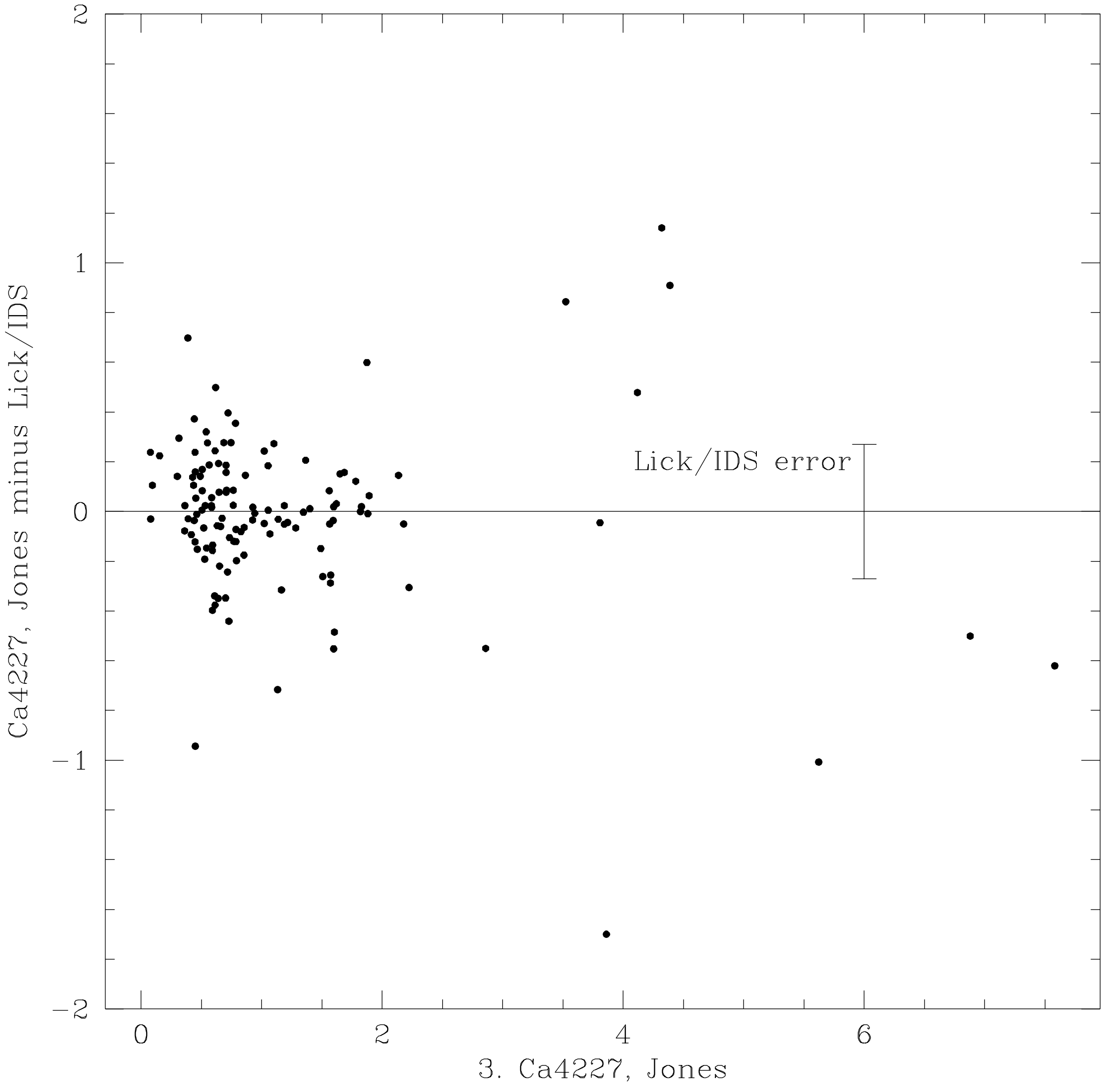

Fig. 8.— Index Ca4227 is shown for 123 Jones stars in common with Lick where the Jones library has been broadened to the Lick/IDS resolution (Table 8). Most of the outliers are KM stars for which the IDS errors are larger than the typical single-observation error shown. More than half of the Lick stars were observed only once. The median Jones−Lick shift is negligible.

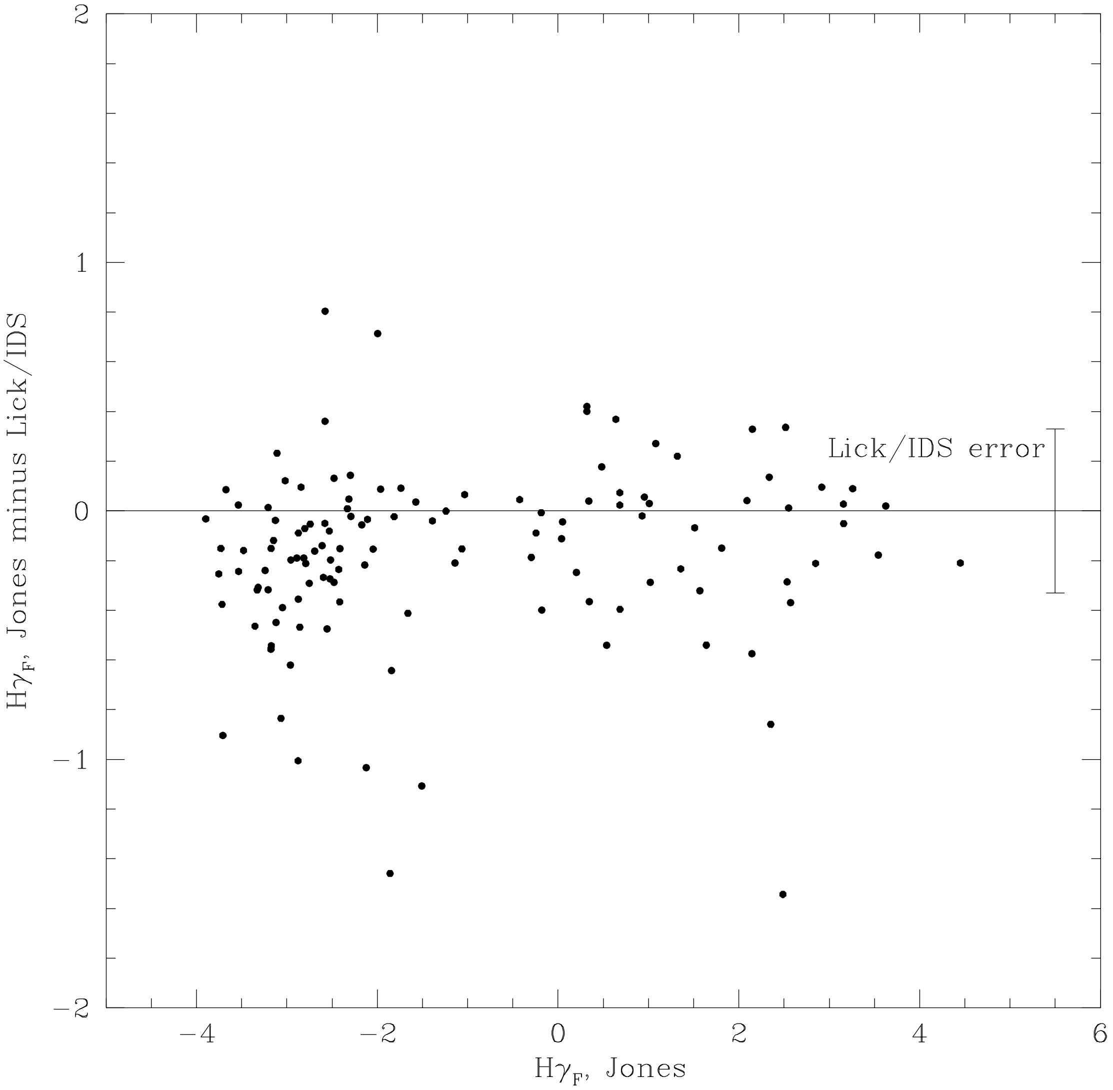

Fig. 9.— Index $H\gamma_F$ is shown for 123 Jones stars in common with Lick where the Jones library has been broadened to the Lick/IDS resolution (Table 8). $H\gamma_F$ is much less sensitive to smoothing than Ca4227. Almost all the outliers are KM stars for which the IDS errors are larger than the typical single-observation error shown. Most of the Lick stars were observed only once. The median Jones−Lick shift is −0.14 Å; not large compared to the IDS error, but very serious for deriving ages for early-type galaxies (about 1.5 Gyr at old ages).

Jones Hβ, G, and Fe4383 indices show shifts almost up to half of an IDS standard error, but these shifts do not show up in the MDM data. In these cases, small changes in smoothing do not fix the problem, and it is not known what the exact cause of the shift is. We do note that these indices are near the edges of the Jones wavelength coverage, but cannot guess if this fact has something to do with the problem. For Fe5015 we are inclined to think that the shift is mostly due to Lick/IDS systematics since the two new data sets agree very well. This also seems to be the case for Hδ as well; both new data sets give a stronger Hδ than does Lick/IDS.

A.3. New data is at lower resolution than Lick/IDS?

Data at somewhat lower resolution than Lick can be corrected back to the Lick resolution with a corresponding increase in uncertainty. An easy way to estimate this effect is to broaden Lick stars to the new resolution and calibrate the effect on the indices. It is desirable but not strictly necessary to have stars in common with the Lick library. The only literature example of this that we are aware of is Davidge (1997).

REFERENCES

Bender, R., Saglia, R. P., & Gerhard, O. E. 1994, MNRAS, 269, 785

Briley, M. M., Smith, V. V., & Lambert, D. L. 1994, ApJ, 424, L119

Burstein, D., Faber, S. M., Gaskell, C. M., and Krumm, N. 1984, ApJ, 287, 586

Davidge, T. 1997, AJ, in press

Faber, S. M., Friel, E. D., Burstein, D., & Gaskell, C. M. 1985, ApJS, 57, 711

Faber, S. M., Trager, S. C., González, J. J., & Worthey, G. 1994, IAU Symposium 164, Stellar Populations (Dordrecht: Kluwer), 255

Fisher, D., Franx, M., & Illingworth, G. 1995, ApJ, 448, 119

González, J. J. 1993, Ph.D. Thesis, Univ. California, Santa Cruz

Gorgas, J., Faber, S. M., Burstein, D., González, J. J., Courteau, S., & Prosser, C. 1993, ApJS, 86, 153

Green, E. M., Demarque, P., & King, C. R. 1987, The Revised Yale Isochrones and Luminosity Functions (New Haven: Yale University Observatory)

Jones, L. A. 1996, Ph. D. Thesis, Univ. North Carolina, Chapel Hill

Jones, L. A., & Worthey, G. 1995, ApJ, 446, L31

Leitherer, C. et al. 1996, PASP, 108, 996

Leonardi, A. J., & Rose, J. A. 1996, AJ, 111, 182

McWillian, A., & Rich, R. M. 1994, ApJS, 91, 749

O'Connell, R.W. 1976, ApJ, 206, 370

O'Connell, R.W. 1980, ApJ, 236, 430

O'Connell, R.W. 1994, in Nuclei of Normal Galaxies: Lessons from the Galactic Center, ed. R. Genzel, (Dordrecht: Kluwer), 255

Osterbrock, D. E. 1980, Astrophysics of Gaseous Nebulae and Active Galactic Nuclei, (Mill Valley, CA: University Science Books)

Penny, A. J., Smith, G. H., & Churchill, C. W. 1992, MNRAS, 257, 89

Rose, J. A. 1985, AJ, 90, 1927

Rose, J. A. 1994, AJ, 107, 206

Salpeter, E. E. 1955, ApJ, 121, 161

Smith, G. H., & Norris, J. 1982, ApJ, 254, 149

Smith, G. H., & Penny, A. J. 1989, AJ, 97, 1397

Statler, T. S. 1995, AJ, 109, 1371

Trager, S. C., Worthey, G., Faber, S. M., González, J. J., & Burstein, D. 1997, ApJS, in preparation

Tripicco, M. J., & Bell, R. A. 1995, AJ, 110, 3035

van der Marel, R., & Franx, M., 1993, ApJ, 407, 525

VandenBerg, D. A. 1985, ApJS, 58, 711

VandenBerg, D. A., & Bell, R. A. 1985, ApJS, 58, 561

VandenBerg, D. A., & Laskarides, P. G. 1987, ApJS, 64, 103

Wheeler, J. C., Sneden, C., & Truran, J. W., Jr. 1989, ARA&A, 27, 279

Worthey, G., Faber, S. M., & González, J. J. 1992, ApJ, 398, 69

Worthey, G. 1994, ApJS, 95, 107

Worthey, G. 1996, in From Stars to Galaxies: The Impact of Stellar Physics on Galaxy Evolution, ed. C. Leitherer, U. Fritze-von Alvensleben, & J. Huchra, ASP Conf. Series vol. 98, (ASP: San Francisco), 467

Worthey, G., Faber, S. M., González, J. J., and Burstein, D. 1994, ApJS, 94, 687

This preprint was prepared with the AAS LaTeX macros v4.0.

Table 2. Index Measurements

(see http://astro.lsa.umich.edu/users/worthey/ for star data.)

HD	name	name	Hδ_A	Hγ_A	Hδ_F	Hγ_F	$N_{\delta A}$	$N_{\gamma A}$	$N_{\delta F}$	$N_{\gamma F}$	qual

Note. — The units of the index measurements in columns 5, 6, 7, and 8 are Angstroms of equivalent width. Columns 9, 10, 11, and 12 indicate the number of observations available for each index. The quality parameter in column 13 is normally one, but is 2 if the errors are judged about twice as large as the Table 1 value, and 3 if the errors are judged three times the Table 1 value or larger. Spectra for HR 296, HR 1726, HR 2047, HR 2503, and HR 2506 were lost subsequent to Faber et al. (1985) and thus do not appear in this table. Most other missing data are due to the spectrograph settings in some runs that excluded the bluest parts of the spectrum. Other data were deleted if irregularities were present in the spectra.

Table 3. Polynomial coefficients for warm stars: $0.75 < \Theta < 1.0$

	Hδ_A	Hγ_A	Hδ_F	Hγ_F
Constant	35.982	99.846	47.273	44.554
Θ_e	-39.599	-180.61	-86.425	-59.657
Θ_e^2	···	74.564	38.573	···
Θ_e^3	···	···	···	13.508
[Fe/H]^2	-0.4963	···	···	···
$(\log g)^3$	-0.01241	-0.02066	···	-0.01438
Θ_e[Fe/H]	···	···	-0.6310	···
Θ_e^2[Fe/H]	-2.8349	-2.5600	···	-0.9540
Fit RMS	1.04	1.82	1.07	1.50

Table 4. Polynomial coefficients for cool stars: $-0.01 < \log\,\Theta < 0.15$

	$H\delta_A$	$H\gamma_A$	$H\delta_F$	$H\gamma_F$
Constant	-4.2019	-7.3344	-1.0345	-1.3462
$\log\,\Theta_e$	-70.590	-47.269	-10.347	-24.410
$\log\,\Theta_e^2$	382.65	···	···	···
$\log\,\Theta_e^3$	···	1.5656×10^3	···	1.1003×10^3
[Fe/H]	-4.8387	-3.7692	-1.3420	-1.3551
$\log\,g$	···	···	···	-0.2741
[Fe/H]($\log\,g$)	···	0.5623	···	0.1976
[Fe/H]$(\log\,g)^2$	0.1443	···	···	···
$(\log\,\Theta_e)^2(\log\,g)$	67.602	···	36.251	···
Fit RMS	1.49	1.73	1.28	1.17

Table 5. Polynomials for very hot and cool stars

Hot stars between $\Theta = 0.38$ and 0.80 ($T_{eff} = 13300$ to 6300 K)
$H\delta_A = -21.300 + 87.328\Theta - 89.3136\Theta^3$
$H\gamma_A = -46.529 + 213.84\Theta - 193.0285\Theta^2$
$H\delta_F = -17.229 + 92.930\Theta - 85.4316\Theta^2 - 0.5143[\mathrm{Fe/H}]$
$H\gamma_F = -20.397 + 106.87\Theta - 98.0065\Theta^2 - 0.2997[\mathrm{Fe/H}]$
M giants between $T_{eff} = 2300$ and 3900 K
$H\delta_A = -44.638 + 0.02945T_{eff} - 4.949 \times 10^{-6}(T_{eff})^2$
$H\gamma_A = -35.040 + 0.02845T_{eff} - 5.728 \times 10^{-6}(T_{eff})^2$
$H\delta_F = -8.528 + 4.334 \times 10^{-3}T_{eff} - 6.195 \times 10^{-7}(T_{eff})^2$
$H\gamma_F = -9.007 + 5.729 \times 10^{-3}T_{eff} - 1.049 \times 10^{-6}(T_{eff})^2$
M dwarfs between $T_{eff} = 2800$ and 4400 K
$H\delta_A = -9.236 + 0.01074T_{eff} - 2.312 \times 10^{-6}(T_{eff})^2$
$H\gamma_A = -8.215 + 8.556 \times 10^{-3}T_{eff} - 2.118 \times 10^{-6}(T_{eff})^2$
$H\delta_F = -14.584 + 9.716 \times 10^{-3}T_{eff} - 1.528 \times 10^{-6}(T_{eff})^2$
$H\gamma_F = -14.155 + 7.846 \times 10^{-3}T_{eff} - 1.242 \times 10^{-6}(T_{eff})^2$

Table 6. Population model predictions

Age (Gyr)	[Fe/H]	Hδ_A	Hγ_A	Hδ_F	Hγ_F
1.5	-0.225	5.208	3.850	3.880	3.435
	0.000	3.864	2.120	3.127	2.528
	0.250	1.771	-0.619	2.097	1.291
	0.500	0.421	-2.303	1.590	0.626
2	-0.225	3.747	2.014	3.085	2.508
	0.000	1.959	-0.340	2.160	1.343
	0.250	-0.030	-3.068	1.264	0.184
	0.500	-1.376	-4.625	0.726	-0.546
3	-0.225	1.995	-0.247	2.163	1.405
	0.000	0.314	-2.639	1.365	0.343
	0.250	-1.192	-4.561	0.689	-0.578
	0.500	-2.481	-5.937	0.214	-1.237
5	-0.225	0.287	-2.790	1.264	0.245
	0.000	-0.632	-3.935	0.875	-0.317
	0.250	-2.335	-5.943	0.165	-1.327
	0.500	-3.691	-7.318	-0.310	-1.969
8	-2.000	6.374	5.109	4.848	4.214
	-1.500	5.034	3.421	3.854	3.280
	-1.000	3.980	2.162	3.219	2.628
	-0.500	0.396	-2.828	1.203	0.152
	-0.250	-0.498	-3.896	0.843	-0.378
	0.000	-1.751	-5.342	0.342	-1.083
	0.250	-3.135	-6.854	-0.192	-1.839
	0.500	-4.325	-7.960	-0.589	-2.326
12	-2.000	5.205	3.525	4.100	3.290
	-1.500	4.056	2.049	3.243	2.504
	-1.000	3.422	1.144	2.789	2.069
	-0.500	-0.303	-3.842	0.823	-0.418
	-0.250	-1.428	-5.074	0.399	-1.025
	0.000	-2.609	-6.323	-0.035	-1.626
	0.250	-4.093	-7.802	-0.587	-2.360
	0.500	-5.234	-8.758	-0.978	-2.768
17	-2.000	4.443	2.509	3.563	2.637
	-1.500	3.581	1.254	2.844	2.007
	-1.000	2.978	0.426	2.554	1.662
	-0.500	-0.974	-4.762	0.490	-0.931

Table 6—Continued

Age (Gyr)	[Fe/H]	Hδ_A	Hγ_A	Hδ_F	Hγ_F
	-0.250	-2.116	-5.893	0.099	-1.491
	0.000	-3.354	-7.091	-0.351	-2.058
	0.250	-4.733	-8.409	-0.830	-2.705
	0.500	-5.704	-9.162	-1.181	-3.037

Table 7. Index metallicity sensitivities

Index	$\left(\frac{\mathrm{d}\ \log\ \mathrm{Age}}{\mathrm{d}\ \log\ Z}\right)_I$
Colors	1.6
Mg_2	1.8
Fe4668	4.9
Hβ	0.6
Hδ_A	1.1
Hγ_A	1.0
Hδ_F	0.9
Hγ_F	0.8

Table 8. Lick/IDS FWHM Resolution.

λ	FWHM
4000	11.5
4400	9.2
4900	8.4
5400	8.4
6000	9.8

Table 9. Median Index Shifts. New minus Lick/IDS.

Index	Jones	MDM
01 CN_1	-0.003	0.007
02 CN_2	-0.004	0.002
03 Ca4227	0.00	0.16
04 G4300	0.17	0.09
05 Fe4383	-0.34	-0.01
06 Ca4455	···	-0.22
07 Fe4531	···	-0.15
08 Fe4668	···	0.13
09 Hβ	0.11	0.01
10 Fe5015	-0.21	-0.26
11 Mg_1	-0.004	-0.043
12 Mg_2	-0.010	-0.049
13 Mg b	0.08	-0.005
14 Fe5270	0.07	0.01
15 Fe5335	0.04	0.05
16 Fe5406	0.04	0.04
17 Fe5709	···	-0.02
18 Fe5782	···	0.00
19 Na D	···	-0.05
22 Hδ_A	0.40	0.41
23 Hγ_A	-0.40	0.18
24 Hδ_F	0.21	0.41
25 Hγ_F	-0.15	-0.03